ResearchGate

See discussions, stats, and author profiles for this publication at: https://www.researchgate.net/publication/356119662

Lattice Polarity Manipulation of Quasi-vdW Epitaxial GaN Films on Graphene Through Interface Atomic Configuration

Article *in* Advanced Materials · February 2022

DOI: 10.1002/adma.202106814

CITATIONS
2

READS
336

21 authors, including:

Fang Liu
Peking University
24 PUBLICATIONS **157** CITATIONS

SEE PROFILE

Zhihong Zhang
University of Science and Technology Beijing
55 PUBLICATIONS **1,928** CITATIONS

SEE PROFILE

Tong Shen
Peking University
8 PUBLICATIONS **13** CITATIONS

SEE PROFILE

Xin Rong
Peking University
51 PUBLICATIONS **819** CITATIONS

SEE PROFILE

Some of the authors of this publication are also working on these related projects:

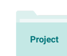
Hyperdoped Semiconductors View project

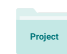
Defect engineering of novel materials by ion beams View project

All content following this page was uploaded by Xin-Qiang Wang on 25 January 2022.

The user has requested enhancement of the downloaded file.

Check for updates

Lattice Polarity Manipulation of Quasi-vdW Epitaxial GaN Films on Graphene Through Interface Atomic Configuration

Fang Liu, Tao Wang, Zhihong Zhang, Tong Shen, Xin Rong, Bowen Sheng, Liuyun Yang, Duo Li, Jiaqi Wei, Shanshan Sheng, Xingguang Li, Zhaoying Chen, Renchun Tao, Ye Yuan, Xuelin Yang, Fujun Xu, Jingmin Zhang, Kaihui Liu, Xin-Zheng Li,* Bo Shen, and Xinqiang Wang**

Quasi van der Waals epitaxy, a pioneering epitaxy of sp^3-hybridized semiconductor films on sp^2-hybridized 2D materials, provides a way, in principle, to achieve single-crystal epilayers with preferred atom configurations that are free of substrate. Unfortunately, this has not been experimentally confirmed in the case of the hexagonal semiconductor III-nitride epilayer until now. Here, it is reported that the epitaxy of gallium nitride (GaN) on graphene can tune the atom arrangement (lattice polarity) through manipulation of the interface atomic configuration, where GaN films with gallium and nitrogen polarity are achieved by forming C—O—N—Ga(3) or C—O—Ga—N(3) configurations, respectively, on artificial C—O surface dangling bonds by atomic oxygen pre-irradiation on trilayer graphene. Furthermore, an aluminum nitride buffer/interlayer leads to unique metal polarity due to the formation of an AlON thin layer in a growth environment containing trace amounts of oxygen, which explains the open question of why those reported wurtzite III-nitride films on 2D materials always exhibit metal polarity. The reported atomic modulation through interface manipulation provides an effective model for hexagonal nitride semiconductor layers grown on graphene, which definitely promotes the development of novel semiconductor devices.

1. Introduction

2D materials represented by graphene are composed of ultrathin atomic layers, and these atomic-scale monolayers (MLs) with an in-plane hexagonal honeycomb lattice are combined through van der Waals (vdW) interactions.[1] Considering their good growth compatibility with hexagonal semiconductors such as wurtzite III-nitrides,[2,3] 2D materials are regarded as an ideal platform for the fabrication of advanced optoelectronic devices beyond the substrate limitation.[4] For instance, transferable III-nitride light-emitting diodes (LEDs)[5] and micro-LEDs[6] have been implemented on graphene, and transferable high-electron-mobility transistors have been prepared on hexagonal boron nitride.[7] Notably, these devices can be transferred from the epitaxial substrate to any other desired substrate with high heat dissipation capacity[8] or flexibility[9]

F. Liu, T. Shen, X. Rong, B. Sheng, L. Yang, D. Li, J. Wei, S. Sheng, X. Li, Z. Chen, R. Tao, X. Yang, F. Xu, K. Liu, X.-Z. Li, B. Shen, X. Wang
State Key Laboratory for Mesoscopic Physics and Frontiers Science Center for Nano-optoelectronics
School of Physics
Peking University
Beijing 100871, China
E-mail: khliu@pku.edu.cn; xzli@pku.edu.cn; wangshi@pku.edu.cn

T. Wang, J. Zhang
Electron Microscopy Laboratory
School of Physics
Peking University
Beijing 100871, China

Z. Zhang
Beijing Advanced Innovation Center for Materials Genome Engineering
Beijing Key Laboratory for Magneto-Photoelectrical Composite and Interface Science
Institute for Multidisciplinary Innovation
University of Science and Technology Beijing
Beijing 100083, China

Y. Yuan
Songshan Lake Materials Laboratory
Dongguan, Guangdong 523808, China

K. Liu, X.-Z. Li, B. Shen, X. Wang
Collaborative Innovation Center of Quantum Matter
Peking University
Beijing 100871, China

K. Liu, X.-Z. Li
Interdisciplinary Institute of Light-Element Quantum Materials
Research Center for Light-Element Advanced Materials
Peking University
Beijing 100871, China

X.-Z. Li, X. Wang
Peking University Yangtze Delta Institute of Optoelectronics
Nantong, Jiangsu 226010, China

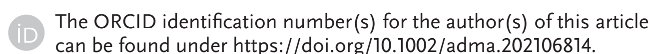
The ORCID identification number(s) for the author(s) of this article can be found under https://doi.org/10.1002/adma.202106814.

DOI: 10.1002/adma.202106814

© 2021 Wiley-VCH GmbH

and so on[10] by breaking the weak coupling interface through a simple mechanical separation method. These results demonstrate an effective method of combining commercial production equipment in the III-nitride industry, such as metal–organic chemical vapor deposition (MOCVD), to intelligently manufacture flexible and/or high-power devices with low cost and high yield.[11] The breakthrough of epitaxial growth of III-nitrides on 2D materials mainly resides on the fine modulation of the weak coupling interface formed by two different hybridized systems,[12] which, in principle, can achieve single-crystal epilayers with preferred atom configurations (i.e., lattice polarity).[13] However, it has not been experimentally confirmed in the case of III-nitride epitaxy on 2D materials until now.

It is known that the sp^2-hybridized graphene surface lacks covalent dangling bonds that can serve as nucleation sites for sp^3-hybridized III-nitrides.[1,2] Perfect vdW epitaxy actually makes the growth of relatively thick (for example, several-µm-thick) III-nitride layers, such as GaN films and device structures, very difficult since epitaxial films are easily peeled off during growth due to the weak interactions at the interface. Therefore, epitaxy of wafer-scale III-nitrides is likely quasi-vdW epitaxy, requiring defects with covalent dangling bonds; however, a lack of sufficient defects often leads to the growth of nanostructures rather than films.[14] To solve this problem, it is necessary to form some artificial dangling bonds on the surface of graphene to improve the nucleation capability of the epitaxial film.[24,25] The quasi-vdW epitaxy of III-nitride films on 2D materials seems to have become a paradigm by first using a pretreatment method such as atomic nitrogen (N) pre-irradiation to form artificial dangling bonds on the surface of graphene and then adopting a high-nucleation-ability AlN buffer layer to improve the crystal quality of the film.[7,15,16] The epitaxial layer and graphene are actually connected in a mixed form of covalent bonds and vdW bonds. This paradigm, on the one hand, provides a unique opportunity to manipulate the interface and thus tune the growth and, on the other hand, leads to an open question of why those films have unique metal lattice polarity and thus lose freedom to fabricate N-polarity based opto-electronic devices.

Here, we report experimental evidence for the quasi-vdW epitaxial growth of high-quality single-crystal GaN films on single-crystal graphene with controllable atomic configuration. For this hexagonal semiconductor, there are two kinds of atomic configurations along the *c*-direction due to the broken inversion symmetry, that is, Ga- and N-lattice polarity, where each Ga atom exhibits 1 or 3 dangling bonds on the growing surface, respectively (Figure S1, Supporting Information). For the first time, these lattice polarities are successfully controlled by forming C—O—N—Ga(3) configuration (for Ga-polarity GaN film) or C—O—Ga—N(3) configuration (for N-polarity GaN film) on artificial C—O surface dangling bonds through atomic oxygen (O) irradiation on transferred trilayer graphene. Due to the universal applicability of this lattice polarity modulation method, it is suitable for different epitaxy methods. Furthermore, we confirmed that a few-nanometer-thick AlN buffer/interlayer leads to unique metal polarity due to the formation of an AlON ultrathin layer, which explains why the reported III-nitride films often exhibit metal polarity. This work can be seen as an effective model of atomic modulation of hexagonal nitride semiconductor films grown on layered graphene through interface manipulation, thereby promoting the industrial development of novel semiconductor devices.

2. Results and Discussion

In this work, we use plasma-assisted molecular beam epitaxy (MBE) to explore the growth behavior of wurtzite GaN films on graphene and thus to build a proper GaN/graphene interface platform. Instead of a graphene monolayer, three-monolayer-thick single-crystal graphene is used to shield the interaction between the epitaxial GaN film and the Al_2O_3 substrate.[3,17] The schematic diagram of the epitaxial growth of GaN films on graphene is shown in **Figure 1**a, which includes four steps: graphene transfer, pre-irradiation, GaN nucleation and GaN growth. First, three graphene monolayers were sequentially transferred to the surface of the Al_2O_3(0001) substrate. Raman scattering measurements (Figure S2a, Supporting Information) confirmed the fine structural quality of the transferred trilayer graphene, where the scattering peak G at 1581.9 cm^{-1} and peak 2D at 2693.1 cm^{-1} derived from graphene are obviously stronger than peak D at 1347.0 cm^{-1} arising from structural defects.[18] Then, atomic O pre-irradiation was applied to partially destroy the hexagonal carbon (C) lattice (Figure S2b, Supporting Information), thereby forming unsaturated C—O dangling bonds on the graphene surface (Figure S2c,d, Supporting Information). Subsequently, by providing Ga atoms and N atoms required for epitaxy, GaN nucleation started from the artificial C—O dangling bonds on the pre-irradiated graphene surface. Finally, GaN nucleation islands continued to grow, coalescence, and eventually form a continuous film with an ordered hexagonal lattice arrangement. Herein, 1 µm-thick single-crystal wurtzite GaN films were grown on the transferred single-crystal trilayer graphene on Al_2O_3(0001) substrates. It was found that there was a 2 nm-thick gap layer composed of in situ atomic O pre-irradiated trilayer graphene, which completely separated the epitaxial GaN film from the Al_2O_3 substrate (Figure S3, Supporting Information). Then, X-ray diffraction (XRD) measurements were performed to evaluate the lattice arrangement of these epitaxial GaN films. In the XRD 2θ–ω scan, the diffraction peak corresponding to the GaN (0002) plane at 34.4° was observed (Figure 1b). It indicates the ordered out-of-plane orientation of the GaN films. In the ϕ-scan for the $(10\bar{1}\bar{5})$ plane of GaN, six peaks with an interval of 60° confirm its in-plane orientation and hexagonal symmetry (Figure 1c). The combination of out-of-plane and in-plane orientations proves that these epitaxial GaN layers all have a regular hexagonal lattice arrangement.[19] It is worth noting that the epitaxial relation between GaN and single-crystal graphene is $(0001)\ [10\bar{1}0]_{GaN} \parallel (0001)\ [11\bar{2}0]_{graphene}$, as shown in Figure S4a–c, Supporting Information. Moreover, the full widths at half maximum of the XRD ω-rocking curves for the (0002) and $(10\bar{1}2)$ planes of the 1 µm-thick GaN film grown on the pre-irradiated trilayer graphene template are 0.29° and 0.35°, respectively (Figure S4e, Supporting Information), which are comparable to those of the film grown directly on the Al_2O_3 substrate. These results indicate that the transferred graphene layer provides the possibility of fabricating single-crystal III-nitride films with high crystal quality.

© 2021 Wiley-VCH GmbH

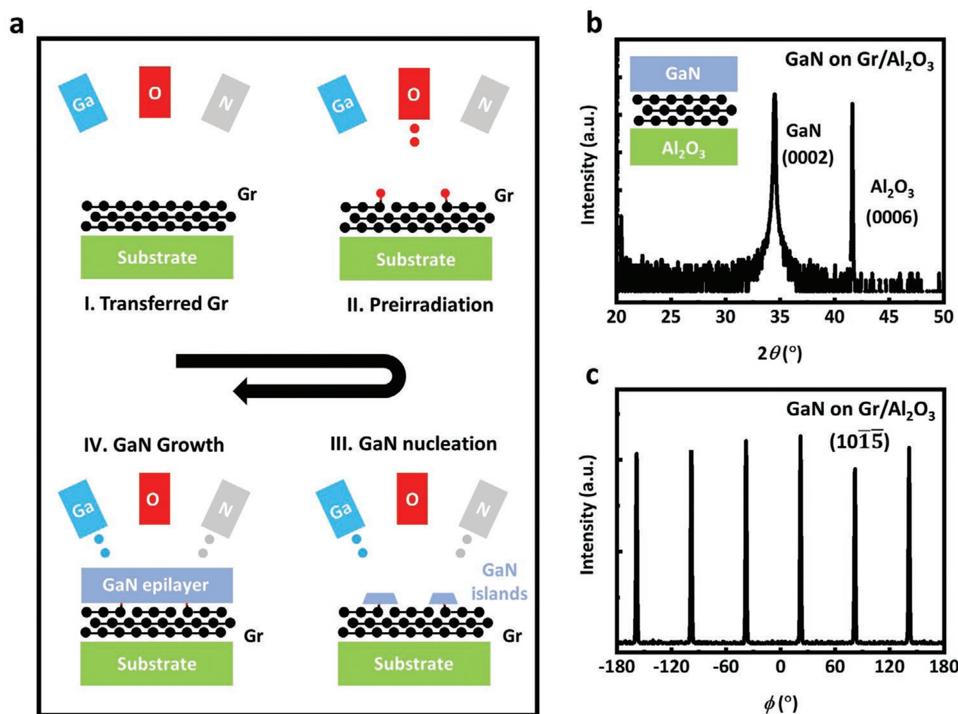

Figure 1. Epitaxial growth of a hexagonal semiconductor GaN film on layered graphene. a) Schematic diagram of the growth process of wurtzite GaN films on graphene (Gr), including transfer of Gr (I), pre-irradiation (II), GaN nucleation (III), and GaN growth (IV). b) XRD 2θ–ω scan of a 1 µm-thick GaN film grown on a trilayer graphene/Al_2O_3(0001) substrate by MBE. c) XRD azimuthal off-axis ϕ-scan for the GaN $(10\bar{1}\bar{5})$ reflection confirming its sixfold symmetry.

Next, we focus on this GaN/graphene epitaxial interface to explore the bonding mechanism of different hybridized materials. The interface bonding of hexagonal semiconductor GaN and graphene mainly depends on two steps shown in Figure 1a of pre-irradiation and GaN nucleation, which actually determine the bonding sequence of Ga or N atoms on the C—O surface dangling bonds on graphene, thereby forming specific interface atomic configurations as initial GaN nucleation islands. Different from the artificial C—N dangling bonds on the graphene surface, which always tend to first bind to Ga atoms to form a C–N–Ga–N(3) configuration and thus start the epitaxy of N-polarity GaN,[20] the unsaturated O atoms in the C—O dangling bonds provide more GaN nucleation options. Density functional theory (DFT) calculations based on this simplified structure (**Figure 2**a) were performed to clarify the interface bonding path and explore the feasible lattice polarity modulation of the epitaxial GaN film on atomic O pre-irradiated graphene. The essence of this simplified structure is the chemical adsorption model of Ga or N atoms on the C—O dangling bonds on the surface of monolayer graphene. More details are provided in the Tables S1 and S2, Supporting Information, and Experimental Section. Four possible interface atomic configurations were considered: 1) one Ga atom combines with the O atom of the C—O bond (C—O—Ga), 2) one N atom combines with the O atom of the C—O bond (C—O—N), 3) one Ga atom replaces the O atom of the C—O bond (C—Ga), and 4) one N atom replaces the O atom of the C—O bond (C—N). The calculated binding energy values of the four possible interfacial bonding paths of GaN on graphene are shown in Figure 2b. The C—O—Ga bond is the strongest (–3.017 eV), indicating that graphene tends to initiate GaN epitaxy by binding one Ga atom on a C—O dangling bond. The C—O—N bond has the second strongest binding energy (–1.967 eV), which means that although the C—O—N bond is not as stable as the C—O—Ga bond, it can still be formed. In contrast, due to the positive binding energy values, the C—N bond (1.762 eV) and C—Ga bond (2.667 eV) are structurally unstable and cannot be formed in principle. Next, the nucleation behavior of GaN on the preferred C—O—Ga and C—O—N bonds was discussed (Figure 2c). The Ga atom in the C—O—Ga bond has three unsaturated bonds, and it is most likely to trigger the nucleation growth of N-polarity GaN on atomic O pre-irradiated graphene by forming the C–O–Ga–N(3) configuration. The difference is that the N atom in the C—O—N bond tends to adsorb three Ga atoms to form the C–O–N–Ga(3) configuration and thus to initiate the epitaxy of Ga-polarity GaN on atomic O pre-irradiated graphene.

Following this principle, we developed a lattice polarity modulation model for epitaxial GaN films on graphene. The core technology is in situ atomic O irradiation of graphene in the MBE chamber at 500 °C. The optimization of the process parameters was briefly discussed elsewhere (Figure S2b, Supporting Information). By prioritizing Ga atoms rather than N atoms during high-temperature (HT) GaN growth, the nucleation and film growth of N-polarity GaN film on pre-irradiated graphene were realized. In detail, the shutter in front of the

 © 2021 Wiley-VCH GmbH

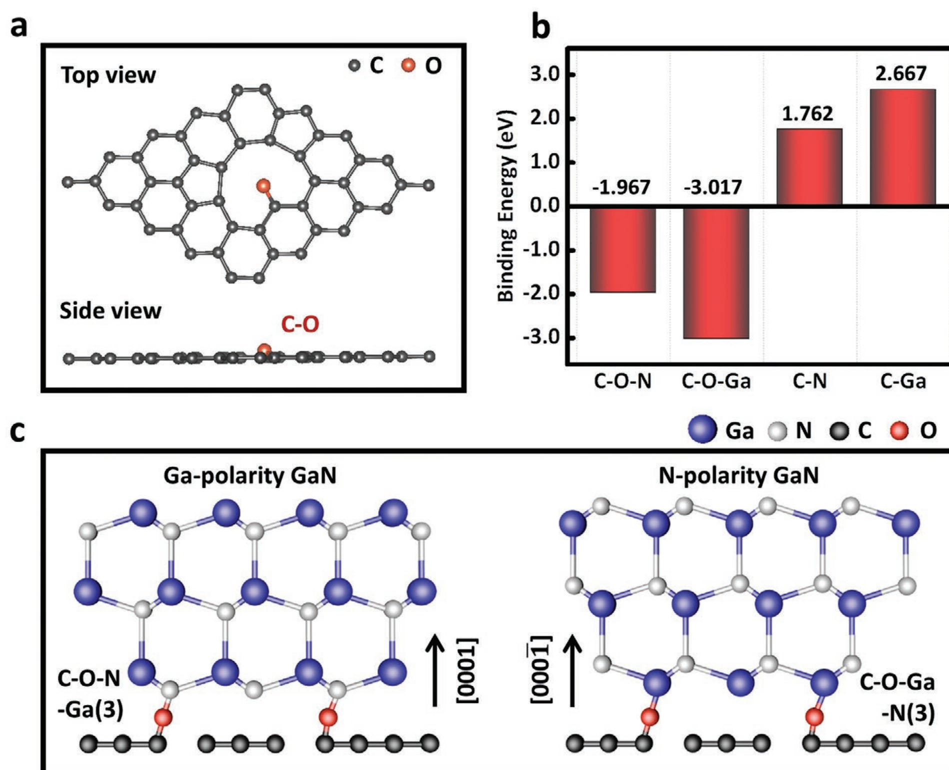

Figure 2. Theoretical calculation of the hexagonal semiconductor GaN/graphene interface bonding configuration. a) Top-view and side-view diagrams of the optimized structure of a single O atom chemisorbed on a graphene monolayer. b) Calculated binding energy values of various cases of one Ga or N atom absorption on a monolayer graphene surface through an unsaturated C—O bond. c) Schematic diagram of the lattice polarity modulation mechanism of wurtzite GaN films grown on graphene through the preferred interface configuration, where the C–O–N configuration tends to adsorb three Ga atoms to from C–O–N–Ga(3) configuration, and the C–O–Ga configuration tends to adsorb three N atoms to from C–O–Ga–N(3) configuration. Herein, the C–O–N–Ga(3) configuration always corresponds to Ga-polarity GaN, and the C–O–Ga–N(3) configuration always corresponds to N-polarity GaN.

Ga source was opened in advance to obtain a 1 nm-thick Ga adsorption layer to protect the epitaxial interface from the destruction of N atoms provided by the N-plasma source. Then, the N-plasma source was stricken, and the epitaxy of GaN started at 780 °C. Its polarity was confirmed by the typical (3 × 3) reconstructed reflection high-energy electron diffraction (RHEED) patterns (Figure S4b, Supporting Information) and the serious deterioration of the surface morphology (**Figure 3**a) after etching with sodium hydroxide (NaOH) solution.[21] In contrast, by opening the shutter in front of the N-plasma source in advance and adopting a 5 nm-thick low-temperature (LT) GaN buffer layer at 500 °C, the epitaxy of Ga-polarity GaN film at 780 °C was also achieved on pre-irradiated trilayer graphene/Al_2O_3 template (Figure S4f, Supporting Information). The Ga-polarity was confirmed by the (1 × 1) unconstructed RHEED patterns (Figure S4c, Supporting Information) and the stable surface morphology after etching with NaOH solution (Figure 3f). It should be pointed out that the quasi-vdW epitaxy of Ga-polarity films requires a more complicated process, due to the fact that the C–O–N configuration is not stable enough (Figure 2b). Therefore, a LT-GaN buffer layer is necessary to protect the C–O–N configuration and subsequent C–O–N–Ga(3) configuration against being broken at high temperature and thus protect the upper Ga-polarity GaN lattice arrangement.[22] Otherwise, the GaN film may eventually exhibit N-polarity due to the dissolution of initial C–O–N/C–O–N–Ga(3) configuration and the formation of other interface bonding such as C–O–Ga–N(3) between GaN and graphene. To probe the interface bonding structure and the origin of the lattice polarity of these GaN films on the graphene template, high-resolution scanning transmission electron microscopy (STEM) measurements were performed on the N-polarity GaN film (Figure 3c) and the Ga-polarity GaN film (Figure 3h). For the N-polarity one, a space gap originated from 3-ML-thick graphene between the GaN film and the Al_2O_3 substrate (Figure 3b). The integrated differential phase contrast (iDPC) STEM images of GaN near the interface region are shown in Figure 3d, where the array of Ga and N atoms along the [000$\bar{1}$] growth direction indicates the N lattice polarity. Moreover, as shown in Figure 3e, this N-polarity lattice arrangement is likely to start from the GaN/graphene interface with a discontinuous monolayer of O atoms (i.e., the C—O dangling bonds on trilayer graphene surface).[23] This is consistent with the calculation results of N-polarity GaN on graphene through the expected C–O–Ga–N(3) configuration (Figure 2c). The following STEM measurements of the Ga-polarity film on trilayer graphene further confirm the interfacial atomic model based on the calculation results (Figure 3g,i). Notably, the Ga lattice polarity of the film results from the GaN/graphene interface, where GaN is most likely to bond with the uppermost graphene through a

© 2021 Wiley-VCH GmbH

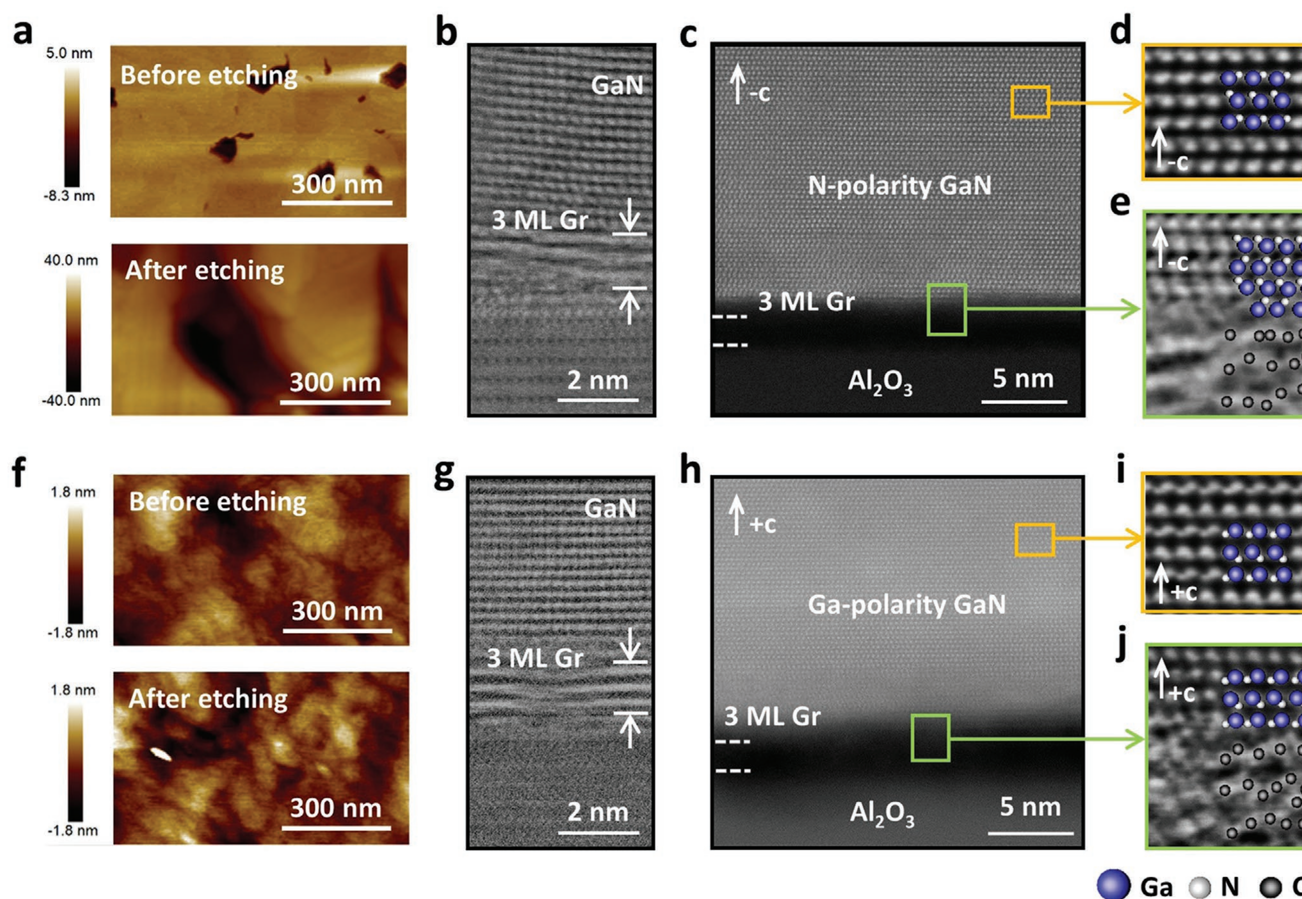

Figure 3. Exploration of the interface atomic structure of epitaxial GaN films on graphene. a) AFM images of a 1 µm-thick epitaxial GaN film grown on a trilayer graphene/Al_2O_3(0001) template via the expected C–O–Ga–N(3) configuration before and after NaOH solution etching. The surface deterioration phenomenon during etching is due to the high surface chemical activity of the N-polarity film. b,c) iDPC-STEM and HAADF-STEM images of the interface atomic structure of this N-polarity film. The adhesion between the graphene and the Al_2O_3 substrate is not perfect, causing the graphene surface to fluctuate, which leads to the tilt of the GaN lattice in some areas. d,e) iDPC-STEM images of the lattice arrangement of this N-polarity GaN film. f) AFM images of a 1 µm-thick Ga-polarity GaN film on a trilayer graphene/Al_2O_3 template through the expected C–O–N–Ga(3) configuration before and after NaOH solution etching. g,h) iDPC-STEM and HAADF-STEM images of the interface atomic structure of this Ga-polarity film. The slightly blurred interface may come from structural damage caused by the high-energy electron beam during STEM measurement. i,j) iDPC images of the lattice arrangement of this Ga-polarity film. Herein, these images (b–e,g–j) viewing both along the [11$\bar{2}$0] orientation of GaN. The [000$\bar{1}$] growth direction of N-polarity GaN is marked as the –*c* direction, and the [0001] growth direction of Ga-polarity GaN is marked as the +*c* direction.

discontinuous O atomic layer (Figure 3j), that is, the expected C–O–N–Ga(3) configuration. Therefore, theoretical prediction (Figure 2) coincides with the experimental results (Figure 3 and Figure S4, Supporting Information), which indicates that the hexagonal lattice of the epitaxial GaN film is determined by the three-monolayer-thick single-crystal graphene layer rather than the substrate and that the lattice polarity is modulated by the interfacial atomic configuration between GaN and graphene. Thus far, we have achieved the quasi-vdW epitaxy of wurtzite GaN films and established a lattice polarity modulation model of epitaxial GaN films on graphene through interfacial atomic configuration.

Notably, this model does not depend on the epitaxy technique. Herein, we also realized the epitaxy of both Ga- and N-polarity GaN films on atomic O-pre-irradiated trilayer single-crystal graphene through MOCVD (Figure S5, Supporting Information). In this case, we used ammonia (NH_3) as the N source and a relatively thick LT-GaN buffer layer to protect the expected interface atomic configuration and prevent it from being destroyed at higher growth temperatures. In addition, we can achieve the separation of quasi-vdW epitaxial GaN film from the Al_2O_3 substrate with the help of thermal release tape (Figure S4f,g, Supporting Information). Because of this lattice polarity modulation model of epitaxial GaN on graphene through interfacial atomic configuration rather than the lattice arrangement of the substrate, we were able to achieve the desired GaN-based epitaxial structures for multifunctional devices on various substrates.

Considering that our MBE system is used for the epitaxy of nitride and oxide semiconductors, the oxygen content in the chamber may be slightly higher than that of the conventional MBE system. From this viewpoint, the growth ambient is somehow close to that of MOCVD. Finally, we would like to answer the open question of why the GaN layer grown by MOCVD on graphene and some other 2D materials with the help of an AlN buffer layer always exhibits Ga lattice polarity.

© 2021 Wiley-VCH GmbH

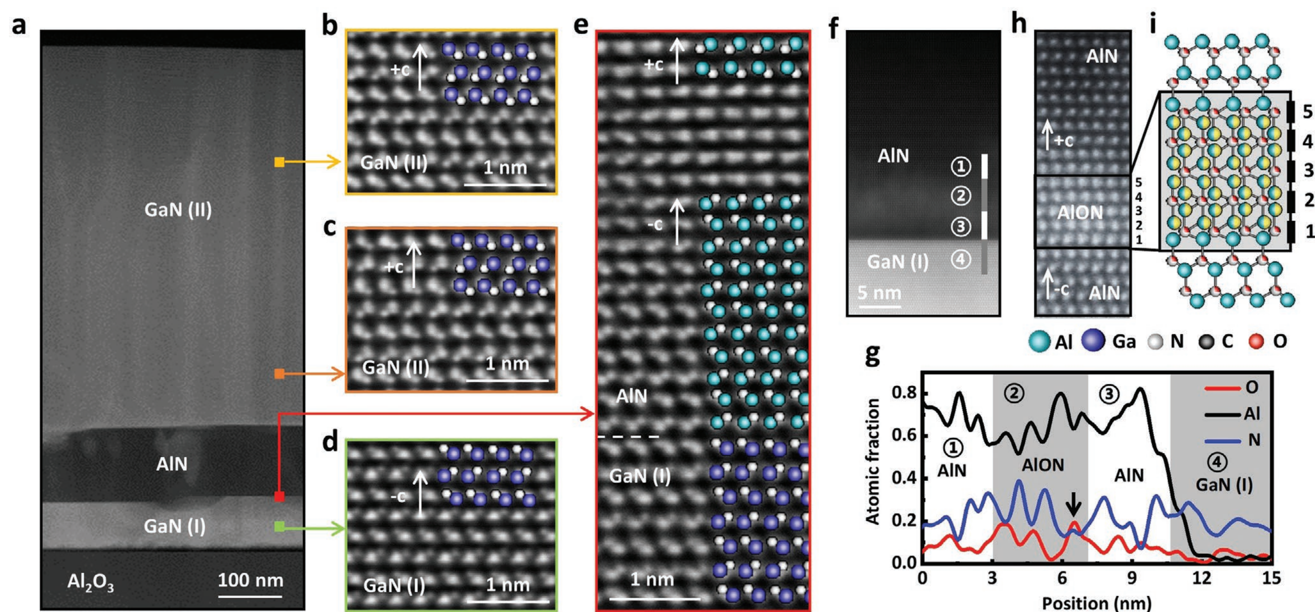

Figure 4. Lattice polarity reversal effect of the AlN interlayer on the upper III-nitride layer. a) HAADF-STEM image of the epitaxial GaN/AlN/GaN sandwich structure on an atomic O pre-irradiated trilayer graphene/Al_2O_3(0001) template through the expected C–O–Ga–N(3) configuration. b–d) iDPC-STEM images of the bottom GaN (I) and upper GaN (II) layers, where the bottom layer has N-polarity and the upper layer has Ga-polarity. e) An iDPC-STEM image of the AlN/GaN interface area, showing the lattice polarity inversion phenomenon existing in the AlN insertion layer. f) A HAADF-STEM image and g) an EDX line scan analysis performed on the AlN/GaN interface showing the enrichment of O atoms in the polarity inversion region of the AlN interlayer. h) A HAADF-STEM image and i) a schematic diagram of the AlN layer above the GaN interface, including the planar inversion domain boundary. Since it is impossible to accurately confirm the ratio of O and N atoms at each position, the N lattice positions in the ideal AlN are filled with two-color small balls to represent AlON. The yellow parts of these Al atom balls indicate possible vacancies. Herein, these images (a–f,h) viewing both along the [11$\bar{2}$0] orientation of GaN.

To eliminate the disturbance of the imperfect graphene surface and slightly disordered AlN nucleation conditions, we designed an experiment using a GaN/AlN/GaN sandwich structure grown on an atomic O-pre-irradiated trilayer graphene/Al_2O_3 template by plasma-assisted MBE (**Figure** 4a). Here, before AlN epitaxy, an 100 nm-thick GaN layer was grown on the transferred trilayer graphene/Al_2O_3 template by the expected C–O–Ga–N(3) configuration to obtain an atomic-scale clear AlN/GaN interface. According to the lattice polarity modulation model of epitaxial GaN discussed above, this structure should has N lattice polarity, similar to the results shown in Figure 3d. However, this method does not seem to be suitable for this GaN/AlN/GaN sandwich structure because the bottom GaN has N-polarity (Figure 4d), while the upper GaN has Ga polarity (Figure 4b,c). In other words, the AlN interlayer reverses the lattice polarity of GaN from N lattice polarity to Ga lattice polarity. Further iDPC-STEM measurements (Figure 4e) show that the lattice polarity of the AlN interlayer is indeed reversed from N- to Al-polarity near the spatial position about 3 nm above the AlN/GaN interface. To illustrate this unusual lattice polarity reversal mechanism, high-angle annular dark-field (HAADF) STEM and energy-dispersive X-ray spectroscopy (EDX) measurements were performed on this AlN/GaN interface. As shown in Figure 4f, there is obvious enrichment of the O composition near the lattice polarity inversion region in AlN compared with GaN or upper AlN, as confirmed by the contrast difference. An EDX line scan performed along the marked direction shows that the average atomic O fraction increased from ≈0.03 (AlN in the white area and GaN in the gray area) to ≈0.08 (AlN in the gray area), as depicted in Figure 4g. However, the atomic N fraction and atomic O fraction exhibited opposite trends with the spatial position. Even at three specific points of AlN in the gray area, the atomic O fraction obviously increased to ≈0.20, and the atomic N fraction decreased to ≈0.14 (marked by the black arrow). The enriched O atoms will tend to partially replace the N atoms in the hexagonal AlN lattice to form a thin AlON layer. The 5-monolayer-thick O-rich AlN layer with an obvious contrast difference with the surroundings (Figure 4h) further proved this viewpoint, where the upper AlN has Al-polarity, and the bottom AlN has N-polarity. Considering the structure of this AlON thin layer,[22,24] we can propose a reasonable lattice polarity reversal model in the AlN interlayer (Figure 4i). Since the precise ratio of O and N components is difficult to directly determine, we used two-color balls to represent nonmetallic atoms. For N-polarity AlN, the higher surface chemical activity facilitates the incorporation of higher fractions of O atoms,[25] which in turn forms a few-nm-thick AlON layer and thus reverses the lattice polarity of the upper AlN to the relatively chemically inert metal polarity. The metal polarity in the AlN layer is mainly related to the incorporation of O atoms from the epitaxial environment, epitaxial substrates, and source materials, which is somehow free of growth equipment. It has been reported that the MOCVD-grown AlN layer on pretreated graphene initially has nitrogen lattice polarity through the C—N dangling bond to form C–N–Al–N(3) configuration, and then reverses to the metal lattice polarity by forming a thin AlON

 © 2021 Wiley-VCH GmbH

layer.[15,19] In other words, in MOCVD growth, a small amount of oxygen will lead to the formation of AlON layer which locks metal lattice polarity of the upper epilayer. Therefore, the lattice polarity modulation of epitaxial GaN on graphene reported in this manuscript provides freedom for fabricating multifunctional devices based on III-nitrides with both kinds of lattice polarities.

3. Conclusion

We have demonstrated the lattice polarity manipulation of quasi-vdW epitaxial GaN on graphene by interface atomic configuration engineering. By using atomic O pre-irradiation and atomic Ga and N supply sequences to form the C–O–N–Ga(3) and C–O–Ga–N(3) configurations, Ga- and N-lattice polarity GaN films were achieved on transferred graphene, respectively. This polarity-control rule is not affected by growth methods such as MBE and MOCVD and is free of either crystalline or noncrystalline substrates. It makes epitaxy of wurtzite III-nitrides with preferred lattice polarity possible on graphene according to objective demands and definitely improves the capability to fabricate more kinds of devices with multiple functions, which is believed to play an important role in next-generation semiconductor devices.

4. Experimental Section

Graphene Synthesis and Transfer: Monolayer single-crystal graphene was grown on a single-crystal Cu(111) substrate by chemical vapor deposition. The growth of graphene was conducted at 1030 °C. The detailed procedure is described in the previous report.[26] Then, trilayer graphene templates were achieved by the poly(methyl methacrylate) (PMMA)-mediated transfer method. Monolayer graphene/Cu was first spin-coated with PMMA (950 K, 4.0 wt% in ethyl lactate). The PMMA/graphene film was pasted onto another graphene/Cu sample after etching the Cu substrate (etchant: 4.0 wt% $(NH_4)_2S_2O_8$ aqueous solution). By repeating the above process again and then removing the Cu substrate, free-standing PMMA/trilayer graphene was obtained. Finally, the dried PMMA/trilayer graphene was transferred onto the Al_2O_3(0001) substrate, and the PMMA was removed by hot acetone (70 °C).

Graphene Pre-Irradiation: The transferred graphene templates were kept at 500 °C in a plasma-assisted MBE chamber with an O-plasma source. Then, 3 min of atomic O pre-irradiation was performed with an O_2 flow rate of 0.8 standard cubic centimeters per minute (sccm) and a radio frequency plasma power of 250 W to form unsaturated C—O dangling bonds on the trilayer graphene surface as nucleation sites for wurtzite GaN epitaxy (Figure S2b, Supporting Information). The C—O dangling bonds formed on the surface of pre-irradiated graphene can be first combined with Ga or N atoms, which makes possible the fine modulation of the interfacial atomic configuration between the GaN film and the graphene.

Theoretical Simulation: DFT calculations were implemented by the Vienna ab initio simulation package code. Projector augmented wave pseudopotentials were used for electron–ion interactions. The generalized gradient approximation was used for the exchange correlation functional as proposed by Perdew–Burke–Ernzerhof. The energy cutoff for plane wave expansion was 600 eV. In the calculation, a $4 \times 4 \times 1$ Γ centered k-point mesh was used, and spin polarization was considered. This monolayer graphene unit cell model contained a 20 Å vacuum layer along the *c*-axis direction to avoid any interactions between periodic images. The lattice parameters of the graphene unit cell were $a = b = 2.468$ Å, $\alpha = \beta = 90°$, and $\gamma = 120°$. More detailed information is provided in Section S6, Supporting Information.

MBE Growth of Wurtzite GaN Films: 1) N-polarity GaN films grown on atomic O pre-irradiated trilayer graphene. In the MBE growth chamber, about 3-ML Ga atoms were first supplied by a thermal evaporation source before HT-GaN epitaxy at 780 °C. Then, the N-plasma source was stricken, and bottom GaN film was deposited at 780 °C. The deposition process is described as follows: turn on the shutters of Ga source for 6 s, the corresponding beam equivalent pressure was 5.5×10^{-7} mbar; then turn on the shutter of N-plasma source for 30 s to provide sufficient N atoms to combine with Ga atoms to form bottom GaN (the N_2 flow rate was 0.25 sccm, and the plasma power was 220 W); repeat the above steps ten times (about 10-monolayer-thick GaN) to protect the expected C–O–Ga–N(3) configuration. Finally, 1 µm-thick N-polarity GaN films were deposited at 780 °C with a growth rate of 3 nm min^{-1}. During GaN epitaxy, the N_2 flow rate was 0.8 sccm, the plasma power was 350 W, and the beam equivalent pressure of the Ga atomic beam was 5.5×10^{-7} mbar. 2) Ga-polarity GaN films grown on atomic O pre-irradiated trilayer graphene. According to theoretical guidance, 5 s of gentle atomic nitrogen treatment was first performed at 500 °C to form an expected C—O—N configuration. Then, a LT-GaN buffer/protection layer (5 nm-thick) was finely deposited at 500 °C, in which the shutter in front of the Ga source was opened 3 s earlier than that of the N-plasma sources. During the abovementioned steps, the N_2 flow rate was 0.25 sccm, the radio frequency plasma power was 220 W, and the beam equivalent pressure of the Ga atomic beam was 5.0×10^{-8} mbar. The small N atomic beam was mainly used to protect these fragile interface states on the graphene surface. Considering the influence of growth temperature on the thermal evaporation rate of Ga atoms on the graphene surface, the Ga beam flux here for LT-GaN epitaxy was also smaller. Subsequently, 1 µm-thick Ga-polarity GaN films were deposited at 780 °C. During GaN deposition, the N_2 flow rate was 0.8 sccm, the plasma power was 350 W, and the beam equivalent pressure of the Ga atomic beam was 5.5×10^{-7} mbar. 3) Epitaxy of AlN interlayer. The AlN interlayer was deposited at 780 °C, and its growth rate was 3 nm min^{-1}. During AlN deposition, the N_2 flow rate was 0.8 sccm, the plasma power was 350 W, and the beam equivalent pressure of the Al atomic beam was 2.5×10^{-7} mbar.

Characterization: The structural quality of transferred graphene was characterized by Raman scattering spectroscopy using a 532 nm laser (CNI MSL-200 mW) as the excitation source and a HORIBA-iHR550 spectrometer. XPS (Kratos, Axis Supra) was performed to quantitatively estimate the chemical composition of graphene before and after atomic oxygen activation. The surface morphology of epitaxial GaN film on the graphene template and the morphology of the GaN film after etching by NaOH solution (10%, AR) at 60 °C for 20 min were measured by AFM in tapping mode (Bruker Dimension ICON-PT). High-resolution spherical aberration-corrected STEM characterization was performed using a FEI Titan Cubed Themis G2 300.

Supporting Information

Supporting Information is available from the Wiley Online Library or from the author.

Acknowledgements

F.L., T.W., Z.H.Z., and T.S. contributed equally to this work. This work was partly supported by the National Key R&D Program of China (No. 2021YFA0716400), the Beijing Outstanding Young Scientist Program (No. BJJWZYJH0120191000103), the National Natural Science Foundation of China (Nos. 61734001, 61521004, 52025023, 11774003, 11934003, 61904002, and 62104010), the Beijing Natural Science Foundation (Nos.

© 2021 Wiley-VCH GmbH

Z200004 and JQ19004), the Guangdong Key Research and Development Program (Nos. 2019B010132001, 2020B010189001, 2019B010931001, and 2018B030327001), the Pearl River Talent Recruitment Program of Guangdong Province (No. 2019ZT08C321), the China National Postdoctoral Program for innovative Talents (No. BX2021007) and the China Postdoctoral Science Foundation (Nos. 2020T130023 and 2020M680234). X.W. thanks Prof. Weikun Ge (Tsinghua University) for helpful discussions. The computational resources were provided by the High-Performance Computing Platform of Peking University, China.

Conflict of Interest

The authors declare no conflict of interest.

Data Availability Statement

The data that support the findings of this study are available from the corresponding author upon reasonable request.

Keywords

epitaxial growth, interface atomic configuration, lattice polarity, layered graphene, wurtzite gallium nitride

Received: August 29, 2021
Revised: October 30, 2021
Published online:

[1] a) A. K. Geim, K. S. Novoselov, *Nat. Mater.* **2007**, *6*, 183; b) X. Z. Xu, Z. H. Zhang, L. Qiu, J. N. Zhuang, L. Zhang, H. Wang, C. N. Liao, H. D. Song, R. X. Qiao, P. Gao, Z. H. Hu, L. Liao, Z. M. Liao, D. P. Yu, E. G. Wang, F. Ding, H. L. Peng, K. H. Liu, *Nat. Nanotechnol.* **2016**, *11*, 930; c) Y. Kubota, K. Watanabe, O. Tsuda, T. Taniguchi, *Science* **2007**, *317*, 932; d) H. Yu, M. Z. Liao, W. J. Zhao, G. D. Liu, X. J. Zhou, Z. Wei, X. Z. Xu, K. H. Liu, Z. H. Hu, K. Deng, S. Y. Zhou, J. A. Shi, L. Gu, C. Shen, T. T. Zhang, L. J. Du, L. Xie, J. Q. Zhu, W. Chen, R. Yang, D. X. Shi, G. Y. Zhang, *ACS Nano* **2017**, *11*, 12001; e) A. Koma, *Thin Solid Films* **1992**, *216*, 72.

[2] a) K. Chung, C. H. Lee, G. C. Yi, *Science* **2010**, *330*, 655; b) J. W. Ben, X. K. Liu, C. Wang, Y. P. Zhang, Z. M. Shi, Y. P. Jia, S. L. Zhang, H. Zhang, W. J. Yu, D. B. Li, X. J. Sun, *Adv. Mater.* **2021**, *33*, 2006761; c) J. H. Park, X. Yang, J. Y. Lee, M. D. Park, S. Y. Bae, M. Pristovsek, H. Amano, D. S. Lee, *Chem. Sci.* **2021**, *12*, 7713.

[3] W. Kong, H. S. Li, K. Qiao, Y. Kim, K. Lee, Y. F. Nie, D. Lee, T. Osadchy, R. J. Molnar, D. K. Gaskill, R. L. Myers-Ward, K. M. Daniels, Y. W. Zhang, S. Sundram, Y. Yu, S. H. Bae, S. Rajan, Y. Shao-Horn, K. Cho, A. Ougazzaden, J. C. Grossman, J. Kim, *Nat. Mater.* **2018**, *17*, 999.

[4] a) J. Kim, C. Bayram, H. Park, C. W. Cheng, C. Dimitrakopoulos, J. A. Ott, K. B. Reuter, S. W. Bedell, D. K. Sadana, *Nat. Commun.* **2014**, *5*, 4836; b) Y. Kim, S. S. Cruz, K. Lee, B. O. Alawode, C. Choi, Y. Song, J. M. Johnson, C. Heidelberger, W. Kong, S. Choi, K. Qiao, I. Almansouri, E. A. Fitzgerald, J. Kong, A. M. Kolpak, J. Hwang, J. Kim, *Nature* **2017**, *544*, 340; c) P. K. Mohseni, A. Behnam, J. D. Wood, X. Zhao, K. J. Yu, N. C. Wang, A. Rockett, J. A. Rogers, J. W. Lyding, E. Pop, X. L. Li, *Adv. Mater.* **2014**, *26*, 3755; d) H. Oh, Y. J. Hong, K. S. Kim, S. Yoon, H. Baek, S. H. Kang, Y. K. Kwon, M. Kim, G. C. Yi, *NPG Asia Mater* **2014**, *6*, e145.

[5] N. Han, T. V. Cuong, M. Han, B. D. Ryu, S. Chandramohan, J. B. Park, J. H. Kang, Y. J. Park, K. B. Ko, H. Y. Kim, H. K. Kim, J. H. Ryu, Y. S. Katharria, C. J. Choi, C. H. Hong, *Nat. Commun.* **2013**, *4*, 1452.

[6] J. Jeong, Q. X. Wang, J. Cha, D. K. Jin, D. H. Shin, S. Kwon, B. K. Kang, J. H. Jang, W. S. Yang, Y. S. Choi, J. Yoo, J. K. Kim, C. H. Lee, S. Lee, A. A. Zakhidov, S. Hong, M. J. Kim, Y. J. Hong, *Sci. Adv.* **2020**, *6*, eaaz5180.

[7] a) N. R. Glavin, K. D. Chabak, E. R. Heller, E. A. Moore, T. A. Prusnick, B. Maruyama, D. E. Walker, D. L. Dorsey, Q. Paduano, M. Snure, *Adv. Mater.* **2017**, *29*, 1701838; b) M. J. Motala, E. W. Blanton, A. Hilton, E. Heller, C. Muratore, K. Burzynski, J. L. Brown, K. Chabak, M. Durstock, M. Snure, N. R. Glavin, *ACS Appl. Mater. Interfaces* **2020**, *12*, 21837.

[8] T. Ayari, S. Sundaram, X. Li, Y. El Gmili, P. L. Voss, J. P. Salvestrini, A. Ougazzaden, *Appl. Phys. Lett.* **2016**, *108*, 171106.

[9] G. Yang, Y. Jung, C. V. Cuervo, F. Ren, S. J. Pearton, J. Kim, *Opt. Express* **2014**, *22*, A812.

[10] a) Y. Kobayashi, K. Kumakura, T. Akasaka, T. Makimoto, *Nature* **2012**, *484*, 223; b) H. Kum, D. Lee, W. Kong, H. Kim, Y. Park, Y. Kim, Y. Baek, S. H. Bae, K. Lee, J. Kim, *Nat. Electron.* **2019**, *2*, 439.

[11] a) Y. Yu, T. Wang, X. F. Chen, L. D. Zhang, Y. Wang, Y. F. Niu, J. Q. Yu, H. T. Ma, X. M. Li, F. Liu, G. Q. Deng, Z. F. Shi, B. L. Zhang, X. Q. Wang, Y. T. Zhang, *Light: Sci. Appl.* **2021**, *10*, 117; b) Y. Qi, Y. Y. Wang, Z. Q. Pang, Z. P. Dou, T. B. Wei, P. Gao, S. S. Zhang, X. Z. Xu, Z. H. Chang, B. Deng, S. L. Chen, Z. L. Chen, H. N. Ci, R. Y. Wang, F. Z. Zhao, J. C. Yan, X. Y. Yi, K. H. Liu, H. L. Peng, Z. Q. Liu, L. M. Tong, J. Zhang, Y. J. Wei, J. M. Li, Z. F. Liu, *J. Am. Chem. Soc.* **2018**, *140*, 11935; c) X. Li, S. Sundaram, Y. El Gmili, T. Ayari, R. Puybaret, G. Patriarche, P. L. Voss, J. P. Salvestrini, A. Ougazzaden, *Cryst. Growth Des.* **2016**, *16*, 3409.

[12] a) D. D. Liang, T. B. Wei, J. X. Wang, J. M. Li, *Nano Energy* **2020**, *69*, 104463; b) J. D. Yu, L. Wang, Z. B. Hao, Y. Luo, C. Z. Sun, J. Wang, Y. J. Han, B. Xiong, H. T. Li, *Adv. Mater.* **2020**, *32*, 1903047.

[13] a) M. Hetzl, M. Kraut, T. Hoffmann, M. Stutzmann, *Nano Lett.* **2017**, *17*, 3582; b) P. Wang, Y. Yuan, C. Zhao, X. Q. Wang, X. T. Zheng, X. Rong, T. Wang, B. W. Sheng, Q. X. Wang, Y. Q. Zhang, L. F. Bian, X. L. Yang, F. J. Xu, Z. X. Qin, X. Z. Li, X. X. Zhang, B. Shen, *Nano Lett.* **2016**, *16*, 1328.

[14] a) H. Yoo, K. Chung, Y. S. Choi, C. S. Kang, K. H. Oh, M. Kim, G. C. Yi, *Adv. Mater.* **2012**, *24*, 515; b) I. M. Hoiaas, A. Liudi Mulyo, P. E. Vullum, D. C. Kim, L. Ahtapodov, B. O. Fimland, K. Kishino, H. Weman, *Nano Lett.* **2019**, *19*, 1649; c) V. Kumaresan, L. Largeau, A. Madouri, F. Glas, H. Z. Zhang, F. Oehler, A. Cavanna, A. Babichev, L. Travers, N. Gogneau, M. Tchernycheva, J. C. Harmand, *Nano Lett.* **2016**, *16*, 4895; d) S. Fernandez-Garrido, M. Ramsteiner, G. H. Gao, L. A. Galves, B. Sharma, P. Corfdir, G. Calabrese, Z. D. Schiaber, C. Pfuller, A. Trampert, J. M. J. Lopes, O. Brandt, L. Geelhaar, *Nano Lett.* **2017**, *17*, 5213; e) J. Jeong, D. K. Jin, J. Cha, B. K. Kang, Q. X. Wang, J. Choi, S. W. Lee, V. Y. Mikhailovskii, V. Neplokh, N. Amador-Mendez, M. Tchernycheva, W. S. Yang, J. Yoo, M. J. Kim, S. Hong, Y. J. Hong, *ACS Appl. Nano Mater.* **2020**, *3*, 8920; f) A. KovACS, M. Duchamp, R. E. Dunin-Borkowski, R. Yakimova, P. L. Neumann, H. Behmenburg, B. Foltynski, C. Giesen, M. Heuken, B. Pecz, *Adv. Mater. Interfaces* **2015**, *2*, 1400230.

[15] Z. L. Chen, Z. Q. Liu, T. B. Wei, S. Y. Yang, Z. P. Dou, Y. Y. Wang, H. N. Ci, H. L. Chang, Y. Qi, J. C. Yan, J. X. Wang, Y. F. Zhang, P. Gao, J. M. Li, Z. F. Liu, *Adv. Mater.* **2019**, *31*, 1807345.

[16] a) J. Ning, C. C. Yan, Y. Q. Jia, B. Y. Wang, Y. Zeng, J. C. Zhang, D. Wang, Y. Hao, *ACS Appl. Nano Mater.* **2020**, *3*, 5061; b) Y. Chen, H. Zang, K. Jiang, J. W. Ben, S. L. Zhang, Z. M. Shi, Y. P. Jia, W. Lu, X. J. Sun, D. B. Li, *Appl. Phys. Lett.* **2020**, *117*, 051601; c) P. Wang, A. Pandey, J. Gim, W. J. Shin, E. T. Reid, D. A. Laleyan, Y. Sun, D. H. Zhang, Z. Liu, Z. H. Zhong, R. Hovden, Z. T. Mi, *Appl. Phys. Lett.* **2020**, *116*, 171905.

 © 2021 Wiley-VCH GmbH

[17] a) S. Zhang, B. Y. Liu, F. Ren, Y. Yin, Y. Y. Wang, Z. L. Chen, B. Jiang, B. Z. Liu, Z. T. Liu, J. Y. Sun, M. Liang, J. C. Yan, T. B. Wei, X. Y. Yi, J. X. Wang, J. M. Li, P. Gao, Z. F. Liu, Z. Q. Liu, *Small* **2021**, *17*, 210098; b) F. Ren, B. Y. Liu, Z. L. Chen, Y. Yin, J. Y. Sun, S. Zhang, B. Jiang, B. Z. Liu, Z. T. Liu, J. W. Wang, M. Liang, G. D. Yuan, J. C. Yan, T. B. Wei, X. Y. Yi, J. X. Wang, Y. Zhang, J. M. Li, P. Gao, Z. F. Liu, Z. Q. Liu, *Sci. Adv.* **2021**, *7*, eabf5011.

[18] J. H. Lee, E. K. Lee, W. J. Joo, Y. Jang, B. S. Kim, J. Y. Lim, S. H. Choi, S. J. Ahn, J. R. Ahn, M. H. Park, C. W. Yang, B. L. Choi, S. W. Hwang, D. Whang, *Science* **2014**, *344*, 286.

[19] Y. X. Feng, X. L. Yang, Z. H. Zhang, D. Kong, J. Zhang, K. H. Liu, X. Z. Li, J. F. Shen, F. Liu, T. Wang, P. F. Ji, F. J. Xu, N. Tang, T. J. Yu, X. Q. Wang, D. P. Yu, W. K. Ge, B. Shen, *Adv. Funct. Mater.* **2019**, *29*, 1905056.

[20] F. Liu, Z. H. Zhang, X. Rong, Y. Yu, T. Wang, B. W. Sheng, J. Q. Wei, S. Y. Zhou, X. L. Yang, F. J. Xu, Z. X. Qin, Y. T. Zhang, K. H. Liu, B. Shen, X. Q. Wang, *Adv. Funct. Mater.* **2020**, *30*, 2001283.

[21] G. Naresh-Kumar, J. Bruckbauer, A. Winkelmann, X. Yu, B. Hourahine, P. R. Edwards, T. Wang, C. Trager-Cowan, R. W. Martin, *Nano Lett.* **2019**, *19*, 3863.

[22] S. Mohn, N. Stolyarchuk, T. Markurt, R. Kirste, M. P. Hoffmann, R. Collazo, A. Courville, R. Di Felice, Z. Sitar, P. Vennegues, M. Albrecht, *Phys. Rev. Appl.* **2016**, *5*, 054004.

[23] Z. P. Dou, Z. L. Chen, N. Li, S. Y. Yang, Z. W. Yu, Y. W. Sun, Y. H. Li, B. Y. Liu, Q. Luo, T. B. Ma, L. Liao, Z. F. Liu, P. Gao, *Nat. Commun.* **2019**, *10*, 5013.

[24] H. Yang, J. G. Lozano, T. J. Pennycook, L. Jones, P. B. Hirsch, P. D. Nellist, *Nat. Commun.* **2015**, *6*, 7266.

[25] a) N. Stolyarchuk, T. Markurt, A. Courville, K. March, J. Zuniga-Perez, P. Vennegues, M. Albrecht, *Sci. Rep.* **2018**, *8*, 14111; b) D. Wang, K. Uesugi, S. Y. Xiao, K. Norimatsu, H. Miyake, *Appl. Phys. Express* **2020**, *13*, 095501.

[26] X. Z. Xu, Z. H. Zhang, J. C. Dong, D. Yi, J. J. Niu, M. H. Wu, L. Lin, R. K. Yin, M. Q. Li, J. Y. Zhou, S. X. Wang, J. L. Sun, X. J. Duan, P. Gao, Y. Jiang, X. S. Wu, H. L. Peng, R. S. Ruoff, Z. F. Liu, D. P. Yu, E. G. Wang, F. Ding, K. H. Liu, *Sci. Bull.* **2017**, *62*, 1074.

© 2021 Wiley-VCH GmbH

View publication stats